



Available online at www.sciencedirect.com

ScienceDirect

Advances in Space Research 76 (2025) 7144-7159

ADVANCES IN SPACE RESEARCH (a COSPAR publication)

www.elsevier.com/locate/asr

GNSS-based synchronization and monitoring of LEO-PNT onboard time

Oliver Montenbruck ^{a,*}, Florian Kunzi ^a, Filipe De Oliveira Salgueiro ^b, Francesco Gini ^c, Miguel Cordero Limón ^b

Deutsches Zentrum f
 ür Luft- und Raumfahrt (DLR), German Space Operations Center (GSOC), M
 ünchener Straße 20, 82234 Weßling, Germany
 European Space Agency (ESA), European Space Research and Technology Centre (ESTEC), Keplerlaan 1, 2201 AZ Noordwijk, the Netherlands
 European Space Agency (ESA), European Space Operations Centre (ESOC), Robert-Bosch-Str. 5, 64293 Darmstadt, Germany

Received 13 August 2025; received in revised form 15 September 2025; accepted 17 September 2025 Available online 20 September 2025

Abstract

For best interoperability, navigation signals transmitted by a positioning, navigation, and timing system in low Earth orbit (LEO-PNT) should be synchronized to the system time scale of an existing GNSS, such as GPS, Galileo, and BeiDou or the Coordinated Universal Time (UTC). Even though an end-to-end assessment of inter-system time offsets can, in principle, be performed based on the analysis of LEO-PNT and GNSS ranging measurements from a joint receiver on ground, this concept lumps multiple error sources and provides only limited insight into the individual contributions. Subject to availability of a GNSS receiver onboard the LEO-PNT satellites, the principle of GNSS time transfer may be used as an alternative to directly determine the difference between the onboard time and a reference GNSS or UTC time scale. The technical requirements for this form of time synchronization are outlined and the individual analysis steps including precise orbit determination (POD) of the LEO satellite and precise point positioning (PPP) processing of GNSS measurements from a timing laboratory are described. For illustration, GNSS measurements from the Sentinel-6A satellite are processed offline in a reference implementation of a real-time navigation system. The resulting "onboard" time scale is then compared to UTC and Galileo System time. Using two fully independent POD/PPP implementations a better than 0.05 ns consistency is demonstrated for the space-to-ground time transfer, which characterizes the achievable precision of the LEO-PNT onboard time monitoring. Making use of Galileo and GPS broadcast ephemerides, the sample Sentinel-6A navigation system is shown to provide an onboard time synchronized to Galileo System Time with RMS errors of 0.75 ns (23 cm) over a continuous 10-day test period. For comparison, 3D RMS position errors of about 9 cm are obtained relative to a precise reference trajectory. The different performance of the onboard time and position determination is mainly attributed to the correlation of clock offsets and carrier phase ambiguities in the realtime navigation filter and appears as a limiting factor for the achievable onboard time synchronization accuracy using GNSS without complementary augmentation data.

© 2025 The Author(s). Published by Elsevier B.V. on behalf of COSPAR. This is an open access article under the CC BY license (http://creativecommons.org/licenses/by/4.0/).

Keywords: LEO-PNT; Time transfer; System time scale; Galileo; UTC; GNSS receiver; Sentinel-6A

1. Introduction

Global navigation satellite systems (GNSSs; Langley et al., 2017) are traditionally based on a moderate number

E-mail address: oliver.montenbruck@dlr.de (O. Montenbruck).

of 24 – 32 satellites transmitting dedicated navigation signals from satellites in medium-altitude Earth orbit (MEOs) at a distance of 25000 – 30000 km from the center of the Earth. Given an increasing number of established and proposed low Earth orbit (LEO) mega-constellations for non-terrestrial communication networks (NTN), positioning, navigation, and timing (PNT) with LEO satellites

^{*} Corresponding author.

(LEO-PNT) has emerged as an important alternative and complement to legacy GNSSs (Prol et al., 2022; Eissfeller et al., 2024). Potential advantages of LEO-PNT include the use of alternative signals and frequencies, improved geometric diversity, potentially stronger signals, and the possibility for new services benefiting from the tight integration of communication and navigation (Ries et al., 2023).

Inspired by the pioneering work of Reid et al. (2018), several commercial providers, including Iridium/Satelles (Riley, 2023), XONA (Youn, 2023), and TrustPoint (Anderson, 2023) in the United States of America as well as Centispace (Mu, 2023; Chen et al., 2023; Li et al., 2024) and Geely (Van Uytsel et al., 2024) in China are offering or preparing dedicated LEO-PNT services. Within Europe, the European Space Agency (ESA) has kicked off an in-orbit demonstration (IOD) mission aiming for first signal transmissions in early 2026 (Priellec et al., 2025) and is working on the next steps towards a potential operational LEO-PNT system.

LEO-PNT has emerged as a driver for highly accurate onboard orbit determination and time synchronization (ODTS) of LEO satellites. Leaving aside the noncooperative tracking of opportunistic signals from LEO communication constellations for ranging and positioning (Stock et al., 2025), the use of GNSS receivers for ODTS is considered as a core of most system architectures currently proposed for LEO-PNT (Giordano et al., 2018; Menzione and Paonni, 2023; Kunzi et al., 2023). This includes both fused navigation concepts (Iannucci and Humphreys, 2022; De Gaudenzi, 2025) based on ranging with the standard communication signals as well as hosted payload architectures (Eissfeller et al., 2024) providing dedicated navigation signals independent of the primary communication services. In both cases, GNSS receivers onboard the LEO satellite are presently considered for real-time orbit determination and timing. While intersatellite ranging may ultimately provide the means for GNSS-independent ODTS, onboard GNSS receivers allow for a fully-integrated system architecture enabling seamless use of MEO and LEO navigation signals in the end-userequipment.

With the above background, the present study addresses the GNSS-based synchronization of LEO-PNT signals to GNSS time and its monitoring using onboard GNSS measurements. In a first step (Section 2), we discuss the basic principles of time as sensed by a GNSS receiver and the generation of a GNSS-aligned onboard time scale in a LEO real-time navigation system. Subsequently, a monitoring concept is developed, which enables comparison of the onboard time scale for the LEO-PNT signal generation against a ground-based time laboratory with traceable links to Coordinated Universal Time (UTC) or a GNSS system time scale (Section 3). The application of the method is illustrated for a sample LEO satellite (Sentinel-6A; Donlon et al., 2021) carrying a stable onboard oscillator and a GPS/Galileo-capable onboard GNSS receiver.

While highly-accurate onboard ODTS and even more the generation of LEO-PNT ranging signals are well beyond the actual mission scope, the Sentinel-6A flight data can be used in a playback real-time navigation filter to generate a smooth and accurate GNSS-aligned time scale representative of a future LEO-PNT system. The quality of this "onboard" time scale is verified against the UTC realization of the Physikalisch-Technische Bundesanstalt (PTB, Braunschweig) and further linked to Galileo System Time (GST) in Section 5. To assess the inherent precision of the monitoring concept itself, two independent realizations using different tool chains and auxiliary data products are utilized. Results from the two implementations are found to agree at the 0.05-ns level, which enables a reliable monitoring of autonomous real-time navigation systems using only GNSS-broadcast ephemerides and offering time synchronization with errors of about 0.75 ns RMS.

2. Receiver and onboard navigation system time

Prior to discussing techniques and procedures for the quantitative assessment of time offsets in the context of LEO-PNT, we briefly review the basic principles of measurement generation and timing inside a GNSS receiver as well as a subsequent real-time navigation system. This section serves to provide the necessary conceptual background concerning timing in a GNSS-based measurement system or a spaceborne GNSS-disciplined oscillator and to introduce relevant notation.

Fundamentally, a GNSS receiver is driven by a local (internal or external) oscillator that provides the reference frequency for down-conversion of the GNSS signals as well as the core-frequency tics for all digital operations. Observations of the received code phase are formed at selected instances ("tics") by correlating a replica of the ranging signal with the incoming signal and latching the instantaneous phase of the code replica within the length of the ranging code. Based on simultaneous processing of the navigation data bit stream, this fractional code phase can be converted into an unambiguous transmit time by adding the frame start time, the duration of full data bits passed since the frame start, and the duration of full ranging codes passed since the start of the latest data bit boundary.

The latching of the code replica is performed synchronously across all available tracking channels, yielding a consistent set of transmit time measurements for all tracked satellites at a common instant defined by the corresponding tic. In parallel to the signal tracking, a receiver time scale is realized within the receiver by associating the measurement tic with an actual time stamp. Pseudorange measurements can then be formed as the product of the speed of light c and the difference of the signal receive ("rx") and transmit ("tx") time:

$$p = c \cdot \left(t_{\text{rev}}^{\text{rx}} - t_{\text{sat}}^{\text{tx}}\right). \tag{1}$$

Here, the subscripts "sat" and "rcv" are used to indicate that the time stamps refer to different time scales, namely the time scale of the transmitting satellite on the one side and the receiver time scale on the other side. Without going into details, carrier-phase observations in a properly designed receiver provide an analogous measurement to the pseudorange, except for an ambiguity that depends on the start of carrier phase tracking and a notably smaller noise level.

In practice, a wide range of options exists concerning (a) the choice of the tic at which the code and carrier phase measurements are latched and (b) the assignment of a receiver time stamp to the measurement tic. Depending on the oscillator stability and accuracy, measurements may be sampled at equally-spaced tic counts (corresponding, for example, to one-second intervals at the nominal oscillator frequency) or irregularly sampled tics to continuously align the latching epoch to the receiver's best estimate of the true integer GNSS-time or UTC second. Likewise, different options apply for the receiver time stamps. These may reflect a linear function of the tic-count assuming a nominal oscillator frequency and initialization with a suitable chosen timestamp at the first tic. Alternatively, time stamps close to the true GNSS or UTC time may be assigned based on the receiver's own estimate of the clock offset and drift obtained as part of the navigation solution. In the case of steered oscillators (such as a voltage-controlled crystal oscillator, VCXO), the oscillator frequency is continuously adjusted based on feedback from the receiver's navigation solution, resulting in an approximately constant number of tics between consecutive measurements, but a potentially higher clock noisy that reflects the precision of the navigation solution.

With very limited exceptions, the internal tic count at the instant of the pseudorange and carrier phase measurements is not reported by common GNSS receivers, thus inhibiting a direct monitoring of the oscillator stability. For use as a LEO-PNT time and frequency source, it must at least be ensured that the receiver latches its measurements at fixed tic-count intervals and does not dynamically change the number of tics between consecutive measurement epochs. Without this precondition, only the instantaneous receiver time offset and thus the true epochs of the individual GNSS measurements may be determined as part of the post-facto validation. In the case of a 1-pulse-per second (PPS) signal aligned with the GNSS measurement epoch it is also possible to determine the deviation of this PPS from the true integer-second of GNSS or UTC time. However, it would not be possible to associate this information with the actual oscillator phase and frequency stability due to the unknown and potentially irregular measurement sampling.

For improved precision of the position and, optionally, timing, the least-squares navigation solution based on epoch-wise pseudoranges is commonly complemented by some form of filtering involving use of carrier phase observations. For the subsequent discussion, it is assumed that LEO-PNT satellites are equipped with such a navigation filter, which may be tightly integrated into the receiver firmware (in the case of specialized space receivers) or oper-

ated on an external processor. Other than terrestrial and aeronautical applications, onboard navigation systems (ONSs) for LEO satellites make use of dynamical or reduced dynamical orbit models to best describe the motion between consecutive epochs and to achieve a refined navigation solution from the available GNSS observations. Aside from an improved determination of the instantaneous spacecraft position this includes an independent estimate of a receiver clock offset parameter. More specifically, this clock offset provides an estimate

$$dt_{\rm rev.ons} \approx t_{\rm rev} - t_{\rm gnss}$$
 (2)

of the difference between the previously defined receiver time scale and the broadcast ephemeris (bce) based realization of the GNSS time scale. It can be used to translate the receiver time scale (as represented by the time tags of the GNSS measurements) to the best onboard knowledge of GNSS time, or, alternatively, the broadcast UTC of a given GNSS, where $\Delta T_{\rm utc-gnss}$ is the predicted offset of UTC and GNSS system time as broadcast by a selected GNSS:

$$t_{\rm ons,gnss} = t_{\rm rev} - dt_{\rm rev,ons} \approx t_{\rm gnss}$$
 (3)

$$t_{\rm ons.utc} = t_{\rm rcv} - dt_{\rm rcv.ons} + \Delta T_{\rm utc-gnss} \approx t_{\rm utc}.$$
 (4)

As indicated by the " \approx "-signs, the above relations represent approximations of the true time scale differences due to various reasons. On the one side, the GNSS system time scale is not directly accessible to normal GNSS users but only via the approximate broadcast orbit and clock information, which is based on forecasts made by the GNSS control segment. Likewise, access to the UTC scale is hampered by the limitations of predicted $\Delta T_{\rm utc-gnss}$ and the aforementioned uncertainty of the GNSS time knowledge. On the other hand, estimates of the receiver clock offset obtained as part of a standalone navigation solution or the onboard navigation system are affected by measurement errors and model errors including errors of the broadcast ephemeris data.

3. LEO-PNT clock monitoring

Conceptually, the time synchronization between a LEO-PNT system and GNSS (or UTC) time can be directly monitored by a properly calibrated receiver on ground, which is able to jointly process ranging signal from both systems. Provided that the time and frequency source, which serves as the basis for the generation of navigation signals onboard the LEO-PNT satellite is itself synchronized to GNSS through an onboard GNSS receiver, this end-to-end comparison can be complemented or substituted by a monitoring of the implemented onboard time reference with respect to the GNSS or UTC time. This comparison builds on established concepts of GNSSbased time and frequency transfer developed for terrestrial receivers, but considers the specific conditions of a fastmoving platform. It is described in further detail in this section.

As discussed above, the onboard navigation system of a GNSS-synchronized LEO-PNT system provides information on the offset between the GNSS receiver time scale and a selected global time scale such as GNSS system time or UTC. Provided that the receiver time scale of the onboard GNSS receiver is derived from the clock beats of the onboard oscillator in a well-defined and traceable manner, a LEO-PNT navigation time scale $t_{\rm lpnt}$ generated from the frequency of the same oscillator, the 1-PPS signal of the onboard GNSS receiver, and the associated onboard navigation system time (Fig. 1) will likewise be traceable to the receiver time scale.

Considering, a LEO-PNT signal that is aimed to be aligned with a global time scale "sys", such as a GNSS time or UTC, the overall time offset between the LEO-PNT time and the system time may be partitioned into a sum/difference of three distinct contributions:

$$dt_{lpnt,sys} = t_{lpnt} - t_{sys}$$

$$= (t_{lpnt} - t_{ons}) + (t_{ons} - t_{sys})$$

$$= dt_{lpnt,ons} + (t_{ons} - t_{sys})$$

$$= dt_{lpnt,ons} - (t_{rcv} - t_{ons}) + (t_{rcv} - t_{sys})$$

$$= dt_{lpnt,ons} - dt_{rev,ons} + dt_{rev,sys} .$$
(5)

Here,

$$dt_{\rm lpnt,ons} = t_{\rm lpnt} - t_{\rm ons} \tag{6}$$

denotes the difference between the LEO-PNT time and the ONS time from which it is derived. It lumps all analog or digital biases that may arise in the synchronization of the navigation signal (as generated by the signal generation unit and transmitted by the LEO-PNT antenna) and the GNSS receiver (represented by its 1-PPS signal). By design, these biases should be stable in time and calibrated at factory level.

The second term, $dt_{rev,ons}$, which has already been introduced above, denotes the receiver time offset as determined by the onboard navigation system and is considered as a known quantity, which can, e.g., be made available for monitoring purposes by the onboard telemetry along with the GNSS receiver observations. The third contribution,

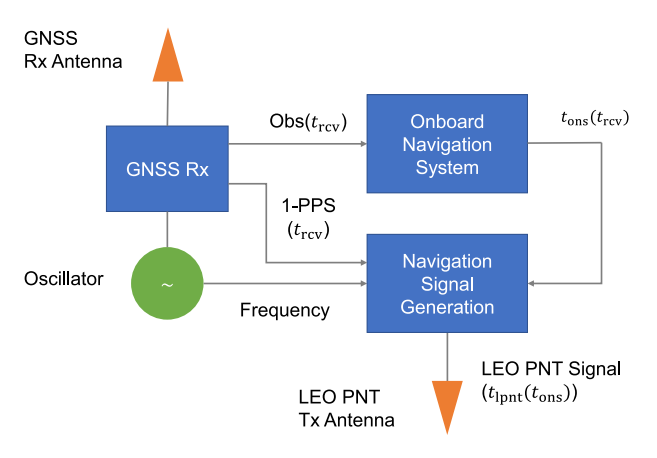


Fig. 1. Conceptual view of LEO-PNT onboard time generation.

$$dt_{\rm rcv,sys} = t_{\rm rcv} - t_{\rm sys} \tag{7}$$

finally denotes the offset between the receiver time scale and the selected system time scale.

The value of $dt_{rev,sys}$ and its variation over time can be determined using a suitably adapted form of GNSS time transfer, provided that joint GNSS observations from a timing laboratory representing the respective system time scale are available. This can, for example, be a permanent reference stations contributing a local realization, UTC(k), to the Coordinated Universal Time. On GNSS-provider level, one of the time reference stations in the mission control segment may be utilized to obtain direct access to the GNSS-specific system time scale.

The conceptual design of the LEO receiver clock offset determination relative to the system time scale is illustrated in Fig. 2. It combines a precise orbit determination (POD; Bar-Sever, 2021) process for the GNSS receiver data of the LEO-PNT satellite and a precise point positioning (PPP; Teunissen, 2021) process for the GNSS observations of the time reference station (TRS). These are primarily intended to obtain the LEO trajectory and the site coordinates, respectively, with utmost accuracy, but only the epoch-wise clock offsets obtained as a "by-product" are used for the present purpose. Here, it is implicitly assumed that the POD and PPP are based on an undifferenced observation model and support provision of the clock solution. This excludes use of traditional double-difference processing but appears to be common practice in most POD and PPP software packages available today.

POD and PPP naturally require different models and auxiliary data for describing the antenna position. This includes sophisticated dynamical models (gravity including tidal variations, macro-models for non-gravitational forces, etc.) for best describing the LEO motion along with attitude dependent center-of-mass offsets of the antenna phase center. Timing receiver antennas, in contrast are treated as static after correction for tidal motion. On the other hand, it is assumed that both processes make use of consistent GNSS observation models as concerns, for example, the GNSS transmit antenna models, phase wind-up corrections, and the Shapiro time delay correction.

Both the POD and PPP processes make use of precise GNSS orbit, clock, and bias products for the constellations of interest. These can readily be obtained from, e.g., the International GNSS Service (Johnston et al., 2017, IGS) and its individual analysis centers (ACs). By using a common set of GNSS products for both the POD and PPP processing, the resulting receiver clock offsets refer to a common time system, which is implicitly defined and realized by the GNSS product provider and depends on the respective processing standard and models. Even though the GNSS product time scale varies from provider to provider and also day to day, this is of no concern for the present analysis. Upon differencing the resulting LEO and TRS clock offsets, the actual GNSS product time scale is

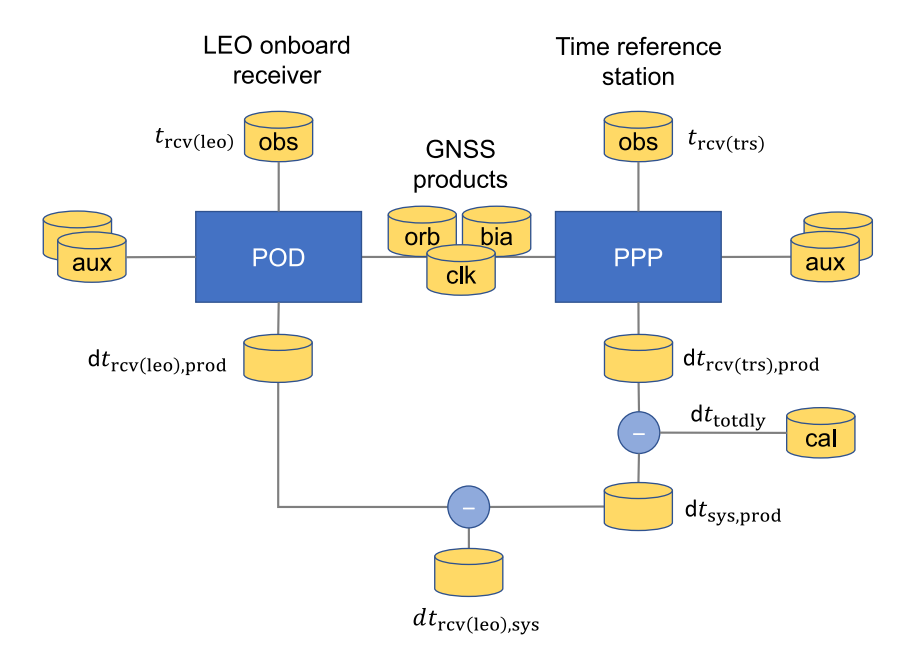


Fig. 2. Process flow for determining the receiver offset from a global system time scale based on GNSS observations (obs), GNSS orbit (orb), clock (clk) and bis (bia) products, as well as auxiliary (aux) and calibration data (cal). The subscript "prod" denotes the time scale of the GNSS clock product.

conceptually canceled and a direct measure of the LEO receiver clock offset relative to the TRS receiver time scale is obtained. Other than common-view time transfer, the POD/PPP processing represents an all-in-view technique than can be used to compare clocks at arbitrary places around the globe and is particularly suitable for LEO-to-ground time transfer. Provided that the GNSS orbit and clock product has itself been determined from a sufficiently dense and globally distributed station network, the achievable precision of epoch-wise POD/PPP clock offset estimates is at the 1 cm (0.03 ns) level (see Section 5), which appears adequate for the envisaged purpose.

As a caveat, we may note that the receiver clock estimation in both the POD and PPP chain depend on the estimation of carrier phase ambiguities in the respective processes. While the precision, i.e. the short-term noise of the estimated clock offsets is driven by the carrier phase quality (including both measurement and modeling errors), the absolute leveling is determined by the amount and quality of code observations. This is particularly relevant when solving for float-valued ambiguities in the overall parameter adjustment process, and may cause errors in the estimated clock offsets with drift and other variations at time scales reflecting the duration of continuous carrier phase tracking arcs. These issues can essentially be overcome through integer ambiguity resolution (Delporte et al., 2008; Petit et al., 2015) in both the POD and PPP processes. Even though the determination of the absolute LEO vs TRS receiver offset will still be affected by the code observations and can only be determined with a granularity of one narrow-lane cycle (approx. 10 cm or 0.3 ns), integer ambiguity time transfer offers the possibility to monitor the LEO clock variation across the day boundaries of common GNSS products.

Another caveat concerns the choice of signal-types for the POD and PPP processing in Fig. 2. In a multi-GNSS context, a primary constellation must be selected which defines the reference GNSS (refcon) for the receiver clock offset estimation. Code (p) and phase (φ) observations for this constellation are essentially modeled as

$$\begin{cases} p \\ \varphi \end{cases} = |\mathbf{r}_{rev} - \mathbf{r}^{sat}| + c \cdot (dt_{rev, prod(refcon)} - dt^{sat}) + \begin{cases} N\lambda \\ N\lambda \end{cases} + \begin{cases} d^{sat} \\ \delta^{sat} \end{cases}, \tag{8}$$

(Hauschild, 2017). Here, only the key contributions required for the present discussion are considered, while other contributions such ionospheric delays, antenna phase patterns, and phese wind-up have been omitted for better transparency. Within the reduced observation model, r and dt denotes the antenna position and clock offset of the receiver and the transmitting satellite, $N\lambda$ denotes the integer-wavelength phase ambiguity, and $d^{\rm sat}$, $\delta^{\rm sat}$ denote the observable specific biases (OSBs). Typically, no receiver biases are included in this model due to a lack of knowledge, and the resulting receiver clock offset estimate is ultimately referenced to a time scale defined by (a) the GNSS orbit/clock/bias product and (b) the selected reference constellation. Observations of a secondary constellation, in contrast would be modeled as

$$\begin{cases}
P \\
\varphi
\end{cases} = |\mathbf{r}_{rcv} - \mathbf{r}^{sat}| + c \cdot \left(dt_{rcv,prod(refcon)} - dt^{sat}\right) + c \cdot dt_{ISB} \\
+ \left\{ N\lambda \right\} + \left\{ d^{sat} \\ \delta^{sat} \right\},$$
(9)

where dt_{ISB} denotes an intersystem bias. It aggregates receiver-specific inter-constellation/inter-signal biases as a

well as product-specific inter-constellation biases that depend on the ISB handling within the GNSS product generation.

Evidently the same primary GNSS must be adopted in the POD and PPP process to ensure a common time reference and enable a differencing of the LEO and TRS receiver offsets w.r.t. to the GNSS product time scale. However, there is no need to harmonize the choice of the reference GNSS for clock offset determination in the POD/PPP process with that of the onboard navigation system. Concerning the choice of signals for the common reference GNSS. common frequencies shall be selected to ensure a rigorous cancellation of satellite code/phase biases as well as the transmit antenna phase patterns and thus avoid the possible errors resulting from an incomplete knowledge of the respective contributions to the determination of the relative clock error between the LEO and TRS receiver. Within a given frequency band, multiple signals may however be transmitted and different tracking modes may be implemented in the respective receivers. In this case, the computed difference between the LEO and TRS receiver clock offsets will contaminated by errors in the intersignal or inter-tracking-modes code biases. As a rule of thumb, these biases can be determined with an accuracy at the level of a few tenths of nanoseconds, which is mainly driven by the lacking separability of satellite and receiver biases in the presence of signal distortions in analog signal generation units and mostly affects the GPS constellation.

In this context, we note that the PPP processing branch in Fig. 2 serves to independently determine the clock offset $dt_{rev(trs),prod}$ of the selected time reference station from the time scale of the precise GNSS products as used in the POD processing of the LEO receiver data. In principle, this PPP process can be skipped, if the respective precise clock product already includes information on the station clock offsets of the given TRS. This is not necessarily ensured in all cases and the set of stations contributing to individual precise GNSS products may vary on a daily basis. Furthermore, station clock offsets are typically given at a reduced sampling rate compared to satellite clocks and refer to a different constellation and signal set than used for the LEO POD. As such, use of the PPP is considered as the most generic approach for determining $t_{rev(trs),prod}$ and can be applied to a larger set of time reference stations than considered in the generation of public GNSS orbit and clock products.

A final step in Fig. 2 concerns the consideration of timing delays related to the antenna and cabling as well as receiver internal delays of the time reference station. Based on the Common GNSS Generic Time Transfer Standard (CGGTT; Defraigne and Petit, 2015) these delays are split into signal/constellation-specific "internal delays" $dt_{\rm intdly}$ (which combines the respective contributions of the antenna and the receiver), the reference delay $dt_{\rm refdly}$ (which describes the offset between the receiver internal clock and the local clock at the station, which can be a realization of

UTC) and the "cable delay" dt_{cabdly} (which specifies the group delay of the antenna cable and connectors). Calibration results for a wide range of UTC(k) laboratories are published by the Bureau International des Poids et Mesures (BIPM), considering, where available, GPS L1/L2, Galileo E1/E5a, and BeiDou B1C/B2a signals (BIBM, 2025).

The difference between the global system time scale, e.g. the UTC(k) of the timing lab hosting the TRS, is then obtained as

$$dt_{\text{sys,prod}} = dt_{\text{rev(trs),prod}} - dt_{\text{totdly}}, \tag{10}$$

where

$$dt_{\text{totdly}} = dt_{\text{intdly}} + dt_{\text{cabdly}} - dt_{\text{refdly}}$$
 (11)

denotes the total delay calibration.

Overall, the LEO receiver time offset from the selected system time is given by

$$dt_{\text{rcv(leo),sys}} = dt_{\text{rcv(leo),prod}} - dt_{\text{rcv(trs),prod}} + dt_{\text{totdly}},$$
 (12)

while the alignment of the onboard navigation time scale to the system time is described by

$$dt_{\text{ons,sys}} = dt_{\text{rcv(leo),prod}} - dt_{\text{rcv(trs),prod}} + dt_{\text{totdly}} - dt_{\text{rcv(leo),ons}}.$$
(13)

4. Timing corrections

4.1. Biases

The time comparison scheme discussed above is based on the processing of pseudorange and carrier phase observations from two receivers. These measurements are based on the difference between the satellite transmit time (as inferred from the modulation and data of the received signal) and the reception time. While group delays in the receiver front end or digital delays in the signal processing chain are typically considered in the receiver design and compensated in the generation of the respective observables as well as the receiver-internal navigation solution, the actual arrival time of a signal in the receiver depends also on external delays such as group delays of the antenna and the external low noise amplifier, as well as cable delays. Unless these delays are made known to the receiver and explicitly taken into account in the measurement generation or applied in the observation model of the ONS, POD, and PPP processes, the resulting clock offset solutions will exhibit a systematic bias reflecting the neglected delay contribution. Likewise, the instant of, for example, a pulse-per second signal will inadvertently be shifted with respect to the desired instant of time.

It should be noted that the presence of unconsidered delays cannot normally be recognized and inferred from the stand-alone GNSS measurements as part of the data analysis and processing. Instead, they need to be obtained from dedicated ground calibrations and have to be consid-

ered either in the measurement generation or the ONS/POD/PPP observation models. Concerning time reference stations in UTC(k) laboratories, the respective delays are normally considered after the fact and applied as calibration corrections to the uncorrected PPP receiver clock offsets (see Fig. 2). For the LEO receiver and onboard navigation systems, no such conventions exist, which hampers a generic description of the respective bias correction scheme.

As a baseline, common concepts for calibration of ground-based timing receivers appear likewise applicable for LEO receivers. This includes both a differential approach using a "golden receiver" (Petit et al., 2000) as well as absolute timing calibrations using a GNSS signal simulator (Proia et al., 2011; Elwischger et al., 2013). An integrated concept for calibration of the LEO GNSS antenna, the antenna cables, and the LEO GNSS receiver using a GNSS simulator and anechoic chamber is, furthermore, described in Valat and Delporte (2020). Following Waller et al. (2019), a one-to-few nanoseconds consistency of the total delay calibrations has been demonstrated for this approach in two independent implementations of this approach by the European Space Agency (ESA/ESTEC) and the Centre National d'Études Spatiales (CNES). However, case-by-case considerations will need to be made for each LEO-PNT mission to ensure a consistent consideration of such calibrations in the GNSS data processing and the comparison of LEO receiver and onboard time scales with the ground reference that exceed the scope of this report. Furthermore, temperature variations representative of the actaul space environment the host satellite may need to be considered for the LEO-PNT GNSS antenna and receiver chain.

4.2. Relativistic effects

Conventional algorithms for GNSS-based positioning and timing provide the receiver/antenna position in an Earth-fixed reference system aligned with the International Terrestrial Reference System. Likewise, the receiver time is determined in a time scale aligned with Terrestrial Time (TT), or, equivalently, International Atomic Time (TAI) and UTC, which represent realizations of the SI second at the surface of the Earth. The overall space-time coordinate system applies in the same way for the receiverinternal single-point positioning and timing as well as real-time or offline orbit/clock solutions computed from the receiver measurements. Furthermore, it equally applies for stationary receivers on ground as well as flying receivers or receivers orbiting the Earth. In a relativistic framework, however, the so-determined TT-aligned coordinate time needs to be distinguished from the proper time τ of the clock, which reflects the time elapsed in a reference system at rest with respect to the respective clock, considering the effects of special and general relativity.

Considering the effects of special relativity, the rate of proper time and the TT-aligned coordinate time differs due the velocity of the orbiting clock as well as the gravitational potential difference between the orbital altitude and the Earth's surface. Following Petit and Luzum (2010), the ratio of the respective time intervals is given by

$$\frac{d\tau}{dt_{\rm TT}} = 1 + L_{\rm G} - \frac{1}{c^2} \left(\frac{|\mathbf{v}|^2}{2} + U(\mathbf{r}) \right),\tag{14}$$

where $L_{\rm G}=6.969290134\cdot 10^{-10}=d(t_{\rm TT}-t_{\rm TCG})/dt_{\rm TCG}$ defines the fractional rate difference of TT and the Geocentric Coordinate Time (TCG), while r and v are the clock's inertial position and velocity relative to the geocenter. For a satellite in low Earth orbit, the dominating contributions to the fractional rate difference of the clock's proper time with respect to TCG are given by

$$\frac{d(\tau - t_{\text{TCG}})}{dt_{\text{TCG}}} = \frac{1}{c^2} \left(\frac{v^2}{2} + U(\mathbf{r}) \right) = L_{\text{LEO}} + \text{periodic terms}$$
(15)

and originate from the mean orbital velocity and the gravitational potential of the Earth's monopole at the mean altitude of the spacecraft. Considering a circular Earth orbit of radius $a=R_\oplus+h$, the mean fractional rate difference amounts to

$$L_{\text{LEO}} = \frac{\overline{d(\tau - t_{\text{TCG}})}}{dt_{\text{TCG}}} = \frac{1}{c^2} \left(\frac{1}{2} \frac{GM_{\oplus}}{a} + \frac{GM_{\oplus}}{a} \right) = \frac{3}{2} \frac{1}{c^2} \frac{GM_{\oplus}}{R_{\oplus} + h}$$

$$\tag{16}$$

where R_{\oplus} , is the Earth's equatorial radius and GM_{\oplus} denotes its gravitational parameter, i.e., the product of the gravitational constant and the mass of the Earth. Depending on the altitude h of the LEO satellite, the mean rate difference

$$\frac{\overline{d(\tau - t_{\rm TT})}}{dt_{\rm TT}} = L_{\rm G} - L_{\rm LEO} \tag{17}$$

of the clock's proper time w.r.t. TT (and thus GNSS time and UTC) ranges about $-0.3 \cdot 10^{-9}$ at h = 300 km to $-0.15 \cdot 10^{-9}$ at h = 1500 km. It may be noted that these values are of similar magnitude as for GNSS satellites, e.g., $L_{\rm G} - L_{\rm GPS} = +0.446 \cdot 10^{-9}$, but of opposite sign.

While an intentional offset of the proper frequency is chosen for the highly stable atomic frequency standards onboard the GNSS satellites to roughly align the clock's coordinate time with TT (Kouba, 2002), the same approach is hardly applicable for lower-grade oscillators which do not exhibit the same clock stability in the presence of changing environmental influences (temperature, magnetic field, ionizing radiation). On the other hand, the actual proper time is of no practical relevance for a LEO-PNT system, when physically disciplining its coordinate time to GNSS time or using GNSS to determine the clock's coordinate time offset from GNSS time.

On top of the mean rate difference, periodic variations in the relative rate of proper time and coordinate time (see Eq. (15)) arise from the varying velocity of the LEO satellite and the varying potential along its orbit. For best accuracy, these need to be evaluated along the actual satellite trajectory and integrated numerically over time to obtain the corresponding clock offset contribution (Wolf and Petit, 1995; Larson et al., 2007). As an alternative, an analytical approximation of the periodic terms in the transformation between proper time and TT has been developed by Kouba (2004). It takes into account the contribution of the monopole and the largest zonal term $J_2 = 1.083 \cdot 10^{-3}$ in the spherical-harmonics expansion of the Earth's gravity field. The satellite orbit is described as a near-circular, perturbed Keplerian orbit, taking into account the first-order perturbations due to Earth-oblateness, which themselves include secular and periodic variations proportional to the J_2 coefficient. Overall, the periodic contributions to the difference of proper time and TCG (or TT, GNSS time, UTC) can then be approximated by

$$(\tau - t_{\text{TCG}})_{\text{periodic}}$$

$$= -\frac{2}{c^2} (\mathbf{r}^T \mathbf{v}) - \frac{3}{2} \frac{1}{c^2} \frac{R_{\oplus}^2}{a^2} J_2 \sqrt{aGM_{\oplus}} \sin^2(i) \sin(2u).$$
 (18)

The first term in this expression depends on the orbital eccentricity and varies with the satellite's eccentric anomaly *E* at a once-per revolution period:

$$-\frac{2}{c^2}(\mathbf{r}^T\mathbf{v}) = -\frac{2}{c^2}\sqrt{aGM_{\oplus}} \cdot e \cdot \sin(E). \tag{19}$$

For GNSS satellites with representative eccentricities of 10^{-2} it dominates the periodic relativistic clock contributions and is used in most GNSSs to translate between coordinate time and a rate-corrected proper time that can be approximated by a polynomial clock offset. However, for LEO satellites with lower orbital radii and representative eccentricities at the 10^{-3} level it is typically of the same order as the Earth-oblateness contribution, which varies twice per revolution with the argument of latitude u, i.e., the angular separation from the ascending node of the orbit. In addition, the Earth-oblateness term varies with the inclination i and is largest for polar orbits that are most widely used for LEO satellites aiming at a global coverage.

As illustrated in Fig. 3 for a sample LEO satellite, the periodic relativistic contributions in the offset of the clock's proper time from the uniform terrestrial time scale exhibit amplitudes at the 1-ns level and periods of half the orbital period. Depending on the stability of the employed onboard oscillator, these variations are likely to be masked by physical variations of the clock frequency and phase in response to varying environmental conditions as the LEO satellite orbits the Earth. Other than for the atomic frequency standards used on GNSS satellites, the consideration of periodic relativistic clock corrections cannot be expected to result in an improved predictability of the

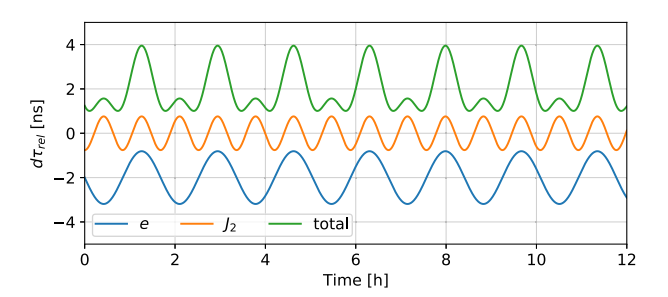


Fig. 3. Eccentricity- and Earth-oblateness-dependent periodic relativistic contributions in the proper time offset from TCG for a sample LEO satellite in polar orbit at 7000km altitude with eccentricity e = 0.001. For clarity, the individual contributions have been offset by ± 2 ns.

LEO onboard clock over (sub-) orbital time scales. At last, it remains at the discretion of the LEO-PNT system design, whether the periodic relativistic contributions of Eq. (18) are removed from the reported LEO clock offsets and need to be added back by the LEO-PNT user, or whether the reported clock offsets directly refer to a TT-aligned coordinate time scale.

5. Sentinel-6A case study

To illustrate the concept of GNSS-based onboard-time monitoring for LEO-PNT satellites, we make use of GNSS measurements collected onboard the Sentinel-6A satellite (S6A; Donlon et al., 2021). The satellite was launched on November 21, 2020 into a circular orbit of 1336 km altitude and 66° inclination. It carries both a GPS-only receiver (Young, 2017, TriG;) and a dual-constellation GPS/Galileo receiver (PODRIX; Peter et al., 2022), which mainly support radio-occultation measurements and precise orbit determination, respectively.

5.1. Data sets and tool chains

For the subsequent analysis, data from the PODRIX receiver have been selected in view of its capability to support both GPS and Galileo tracking. A total of ten days covering October 26 to November 4 (i.e., day of year (DoY) 300–309) of 2024 are considered, which takes advantage of the almost completed Galileo constellation.

Other than for common GNSS receivers, pseudorange and carrier phase observations from the PODRIX receiver are constructed on ground from raw values of the code phase as well as the phase of the down-converted carrier at the intermediate frequency. This involves the free choice of a receiver time scale as defined by the time stamps assigned to the individual GNSS measurement epochs. For the present work, a receiver time scale is derived from the nominal 10-MHz clock beats of an ultra-stable oscillator (USO) by adding a 4th-order clock polynomial, which aligns the resulting receiver time scale to the GNSS-based navigation solution of the receiver itself on a daily basis. S6A observation data referred to a receiver time scale of

this type are generated by the Copernicus Precise Orbit Determination Service (CPOD; Fernandez et al., 2024) from the raw receiver telemetry and shared through the Copernicus Data Space Ecosystem (CDSE) in the REceiver INdependent eXchange version 3 format (RINEX; Romero, 2017).

By design, the adopted S6A receiver time scale closely follows a global atomic time scale over the daily interval. This is illustrated in Fig. 4, which shows the receiver clock offset $dt_{rcv(s6a),utc(ptb)}$ relative to UTC(PTB) as determined in an ambiguity-fixed precise orbit determination using DLR's GNSS High Precision Orbit Determination Software tools (GHOST; Calliess et al., 2024). Despite the good overall stability of the employed USO and the prealignment of the receiver time with a GNSS time scale, half-daily variations of roughly quadratic nature and distinct peaks at selected epochs separated by an orbital period may be recognized. These relate to regular changes in the oscillator drift rate caused by ionizing radiation accumulated during passages of the South Atlantic Anomaly, which take place in two groups of consecutive orbits separated by half a day and have previously been noted on other remote sensing satellites using a similar oscillator (Montenbruck et al., 2021).

Compared to these variations that reflect the inherent stability of the S6A USO, periodic contributions in the coordinate-time/proper- time transformation are roughly one order of magnitude smaller. On the given day, the eccentricity and Earth-oblateness effects described in Section 4.2 add up to roughly 10 cm (0.3 ns) amplitude with a combination of once-per-revolution and twice-per-revolution harmonics. Despite their moderate size, these contributions have been removed in Fig. 4 to best illustrate the natural oscillator stability.

To assess and characterize the processing scheme of Fig. 2 for determining the offset of the onboard receiver time from an international terrestrial time scale, two fully independent POD/PPP processing chains have been implemented and evaluated for this study. These are based on the GNSS High Precision Orbit Determination Software tools (GHOST; Calliess et al., 2024) and the ESA Precise Navigation Software (EPNS), evolution of the NAvigation Package for Earth Orbiting Satellites (NAPEOS; Springer, 2009), respectively. Aside from the use of distinct software packages, the two processing chains make use of different

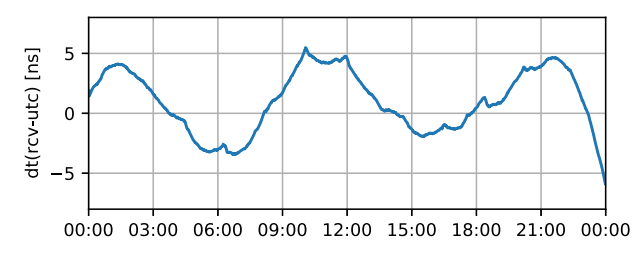


Fig. 4. Offset of the Sentinel-6A PODRIX receiver time from UTC(PTB) for October 30, 2024.

GNSS orbit, clock and bias products. While the final products of the Center for Orbit Determination in Europe (CODE; Dach et al., 2023) are used within the DLR processing chain, a dedicated set of Galileo-only products has been computed by the European Space Operations Center (ESOC) following the standards of their multi-GNSS products (Gini et al., 2024). In this way, we demonstrate that the space-to-ground time transfer results are essentially unaffected by both the choice of tools and the choice of auxiliary GNSS data products.

For added diversity, a combined Galileo/GPS processing is, performed in the first branch, while a Galileo-only processing is selected for the second branch. However, Galileo E1/E5a signals are consistently applied in all cases (POD and PPP of both chains) for the receiver clock offset determinations to enable an unbiased link to Galileo System Time. In the case of dual-constellation processing (chain A), GPS observations contribute to the orbit and position estimation, but do not directly affect the estimated receiver clock offset due to the estimation of epoch-wise inter-system biases (ISB). For further information, a high-level overview of data and models used in the two POD/PPP chains is provided in Table 1.

As the reference station for UTC access, we made use of the PTBB0DEU station of the Physikalisch-Technische Bundesanstalt (PTBB), which acts as the national German time laboratory and is a key contributor to the Coordinated Universal Time. The respective observation data in RINEX format are publicly shared through data centers of the IGS. Calibration data linking the raw receiver time to UTC(PTB) are provided in BIBM (2024) for both GPS L1/L2 and Galileo E1/E5a signals.

5.2. Real-time navigation using GNSS observations and navigation data

To illustrate the monitoring of time synchronization in a representative on-board navigation system, Sentinel-6A flight data were processed in a play-back real-time navigation software (Montenbruck et al., 2022; Kunzi and Montenbruck, 2022) using Galileo and GPS observations along with the respective broadcast navigation data. While both constellations contribute to the overall quality of the position solution, the clock offset estimation is based Galileo observations in the filter configuration chosen for this study and therefore tied to the Galileo System time (GST). The GPS measurements model, on the other hand, involves an additional ISB that is estimated as a white noise parameter at each epoch. Dynamical models and reference frame transformations are tailored for the needs of real-time navigation with broadcast ephemerides, while keeping the algorithmic complexity and computational effort compatible with actual onboard processor capabilities (Kunzi et al., 2023). Further details on the architecture and modeling of the play-back navigation filter and its application to Sentinel-6A are given in Table 2 and Montenbruck et al. (2022). Broadcast navigation messages

Table 1
Data and models for POD/PPP time transfer.

Step	Item	Chain A (DLR)	Chain B (ESA)
LEO POD	Software	GHOST RDOD_AR (Reduced Dynamic Orbit Determination with ambiguity resolution)	ESA Precise Navigation System (EPNS_1.2.1)
	Observations	Code and phase ionosphere-free linear combination; Galileo (1C,5Q), GPS (1C,2L for Block IIR-M, IIF, III; 1 W,2 W for Block IIR); 30-s sampling, 24-h arcs	Code and phase ionosphere-free linear combination; Galileo (1C,5Q)
	GNSS products	COD0OPSFIN (orbit, clock, code/phase biases)	ESA3MGNFIN (orbit, clock, code/phase biases)
	GNSS antenna model	igs20.atx	esa23.atx (satellites), igs20 (receivers)
	Ref. frame transform.	IERS2010 conventions; ITRF2020 geocenter motion	IERS2010 conventions
	Earth rotation	IGS0OPSFIN series	IERS Bulletin A
	Dynamical models	Earth gravity (GOCO06S, 70×70);	Earth gravity (EIGEN.GRGS.RL05.MEAN-FIELD with qudratic
		solid Earth tides (IERS2020), pole tides (IERS2018), ocean tides (FES2014b, 30×30);	mean pole and drift/annual/semi/annual piece wise linear terms, 80×80 ; Earth tides (IERS2010), pole tides (IERS2010), ocean tides
		luni-solar gravitation (point mass; analytical ephemerides) solar radiation pressure (macro-model, conical shadow model); Earth	(FES2022, 80×80); atmospheric gravity and tides (AOD1B RL06); third body Sun, Moon, planets (DE405); solar radiation pressure
		radiation pressure (CERES); drag (NRLMSISE-00); relativity (post-	(macromodel, conical shadow model), Earth (albedo and IR) radiation
		Newtonian correction)	pressure (macro-model, CERES maps); atmospheric density (msise90)
	Receiver antenna	Phase center and pattern from DLR in-flight calibration	sen20_2257.atx
	Observation model	phase wind-up; space-time curvature correction; periodic relativistic clock correction	phase wind-up; space-time curvature correction; periodic relativistic clock correction
	Estimation	Batch least-squares	Batch least-squares
	Parameters	Epoch state vector; solar radiation pressure scale factor; piecewise- constant empirical accelerations in radial, along-track, cross-track direction; carrier-phase ambiguities (with WL/NL fixing); epoch-wise clock offsets (Galileo) and inter-system biases (GPS)	Epoch state vector; atmospheric drag scale factor; 18 sets of piece-wise constant empirical accelerations 1/rev in along-track (constant/sine/cosine) and cross (sine/cosine) direction; carrier-phase ambiguities with WL/NL fixing; epoch-wise clock offsets
ррр	G 6	. , , , , , , , , , , , , , , , , , , ,	
	Software Observations	GHOST MCP (Multi-Constellation Positioning) Code and phase ionosphere-free linear combination, Galileo (1C,5Q), GPS (1C,2L; 1 W,2 W);	ESA Precise Navigation System (EPNS_1.2.1) Code and phase ionosphere-free linear combination, Galileo (1C,5Q);
		30-s sampling, 24-h arcs	30-s sampling, 24-h arcs
	GNSS products	COD0OPSFIN (orbit, clock, code/phase biases)	ESA3MGNFIN (orbit, clock, code/phase biases)
	Antenna model	igs20.atx	esa23.atx (satellites), igs20.atx (receivers)
	Site motion	solid Earth and pole tides (IERS2010/18)	solid Earth, pole tides (IERS2010), ocean loading (EOT11A)
	Observation model	phase wind-up; GPT/GMF a priori troposphere model; elevation cut-	phase wind-up; GPT/GMF a priori troposphere model; elevation cut-
		off angle 10°, elevation-dependent weighting scheme; space–time curvature correction	off angle 10°, elevation-dependent weighting scheme; space-time curvature correction
	Estimation	Batch least-squares	Batch least-squares
	Parameters	Site position (static); zenith troposphere delay correction (piece-wise linear, once per 2h); carrier phase ambiguities (with WL/NL fixing); epoch-wise clock offsets (Galileo) and inter-system biases (GPS)	Site position (static); zenith troposphere delay correction (piece-wise linear, once per 1 h), North and East gradients as linear parameter, once per day; carrier phase ambiguities (with WL/NL fixing); epochwise clock offsets (Galileo)

Table 2
Data and models for play-back real-time navigation.

Item	Description
Software	RTNAVI
Observations	Code and phase; Galileo (1C, 5Q), GPS (1C, 2L for Block IIR-M, IIF, III; 1 W, 2 W for Block IIR); 60-s sampling; 10-d arc (continuous)
GNSS orbit and clock	GPS L1 C/A Legacy NAVigation (LNAV) message, Galileo E5a Free NAVigation message (FNAV)
Code biases	GPS L2C Civil Navigation message (CNAV)
Reference frame	EME2000
Transformations	IERS1996 conventions
Earth rotation	GPS CNAV
Dynamical models	Earth gravity (GGM01S, 50×50); solid Earth tidess (k_2); solar radiation pressure (cannon ball; cylindrical shadow model); drag (cannon ball; Harris-Priester density model); Earth radiation pressure (constant radial acceleration) lunisolar gravity (point mass; simplified analytical ephemerides); empirical accelerations (RTN)
Numerical integration	5th-order Dormand-Prince; 4th-order interpolant
Receiver antenna	Phase center and pattern from in-flight calibration
Observation model	1st-order ionosphere correction; phase wind-up; periodic relativistic clock correction
Estimation	Extended Kalman filter (EKF)
Parameters	Position and velocity; solar radiation pressure and drag scale factors; empirical accelerations (exponentially correlated random variable); clock offset (Galileo; white noise) and ISB (GPS; white noise); pseudo-ambiguities (float; white noise)

of GPS and Galileo including orbit and clock information as well as differential code biases and Earth rotation parameters were obtained from the BRD4 multi-GNSS navigation data files collected by the IGS on a daily basis (Montenbruck and Steigenberger, 2022).

Depending on the quality of the respective broadcast ephemerides, the employed algorithms offer a representative 3D RMS position accuracy at the one to few decimeter level for typical LEO satellites, which is well consistent with the performance achieved in other studies (Hauschild and Montenbruck, 2021; Darugna et al., 2022; Li et al., 2023) and can serve as a practical reference for the expected accuracy of fully autonomous, unaugmented precise on-board navigation solution of future LEO-PNT satellites. In the specific test case of this study, the simulated real-time navigation solution exhibits a 3D RMS position error of 9.2 cm in comparison with the CPOD combined precise orbit determination result (Fernandez et al., 2024). This value is dominated by the contribution of the along-track component (7.3 cm RMS), while the radial and crosstrack errors are roughly a factor of two smaller (Fig. 5).

Complementary to the center-of-mass position of the host vehicle, the (simulated) onboard navigation system provides an estimate $dt_{\rm rev,ons}$ of the receiver clock offset relative to the broadcast realization of the Galileo system time (see Section 2). Based on this estimate, the epochs of the GNSS measurements and associated event markers (such as 1-pulse-per second signals) can be referred to an onboard approximation of the chosen GNSS system time scale. The S6A receiver-time-minus-ONS-time offset $dt_{\rm rev,ons}$ obtained with the present sample implementation of a real-time navigation system for a selected test day is shown in Fig. 6. It resembles the receiver-time-minus-UTC(PTB) offset previously shown in Fig. 4, but exhibits increased short-term variations that reflect the quality of the GNSS-based onboard time determination as well as a

systematic bias, which roughly reflects the offset between UTC(PTB) and the broadcast realization of Galileo system time. A quantitative assessment of the onboard time realization achieved by the real-time navigation algorithm selected for this study is provided in the following subsection.

5.3. Space-to-ground time transfer

As discussed in Section 3 and Fig. 2, the combination of a precise orbit determination using onboard GNSS measurements and the precise point positioning of a suitable time reference station provides the basic link between the various onboard time scales and terrestrial time scales such as UTC or GNSS time. The consistency and quality of the POD and PPP processes directly affects the achievable performance of the space-to-ground time transfer and thus the precision with which the LEO-PNT onboard time can be monitored via onboard GNSS measurements. With this background, we first assess the consistency of the Sentinel-6A receiver time offsets from a UTC(k) laboratory, here UTC(PTB), as determined in two fully independent state-of-the art POD/PPP software systems using different intermediate GNSS orbit and clock products.

For this purpose, precise orbit and clock solutions of Sentinel-6A were first computed on a daily basis over the 10-day analysis period using the DLR (chain A) and ESA (chain B) POD software along with the COD0OPS-FIN and ESA3MGNFIN orbit and clock products. In a second step, daily precise point positioning solutions for the PTBB receiver (i.e., IGS station PTBB0DEU) were computed in the two chains using the respective PPP software modules along with the respective GNSS orbit and clock products. Differences (B–A) between the two chains were then evaluated to assess the consistency of the different implementations and auxiliary data (Fig. 7). Due to the

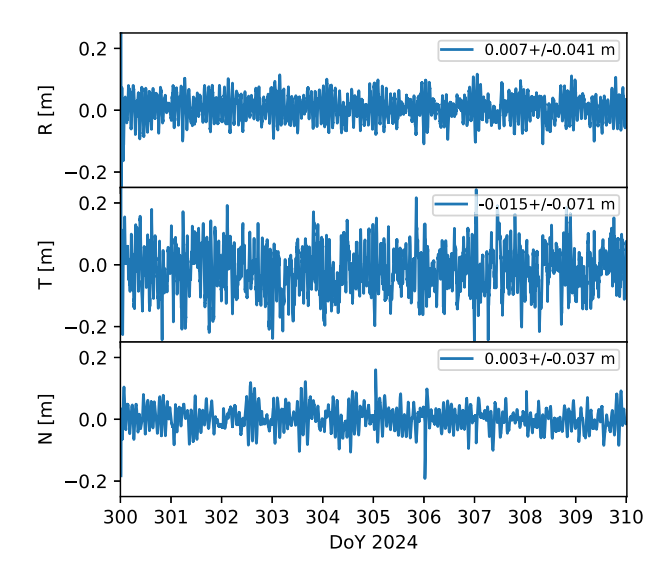


Fig. 5. Position errors of Sentinel-6A play-back real-time navigation solution in radial (R), along-track (T), and cross-track (N) direction. Labels provide the mean \pm standard deviation of the respective time series.



Fig. 6. Offset of the Sentinel-6A PODRIX receiver time from the onboard navigation system time as estimated by the play-back real-time navigation system for October 30, 2024.

use of distinct GNSS orbit and clock products, different clock offsets are obtained in the two chains in both the Sentinel-6A receiver POD and the PTBB PPP solutions. Differences between chain A and B range from roughly 2-4 ns in the period of interest and reflect essentially the inconsistent system time scales of the COD0OPSFIN and ESA3MGNFIN clock products. These are individually tied to a GNSS reference station driven by a highly stable hydrogen maser, but the selection of the reference station may vary on a daily basis in the case of the COD0OPSFIN product, whereas a fixed station (ESOC) is used in the other case. As such, drift changes and day-boundary discontinuities of up to 0.5 ns are encountered in the system time scale difference of the two GNSS products. These can readily be recognized in both the differences of the estimated S6A receiver cock offsets between chain A and B (Fig. 7, top) and the corresponding PTBB clock offset differences (Fig. 7, center).

However, the different product time scales fully cancels when evaluating the S6A receiver offset from UTC(PTB), in which case highly consistent results are obtained for the two chains (Fig. 7, bottom). In total, the RMS differ-

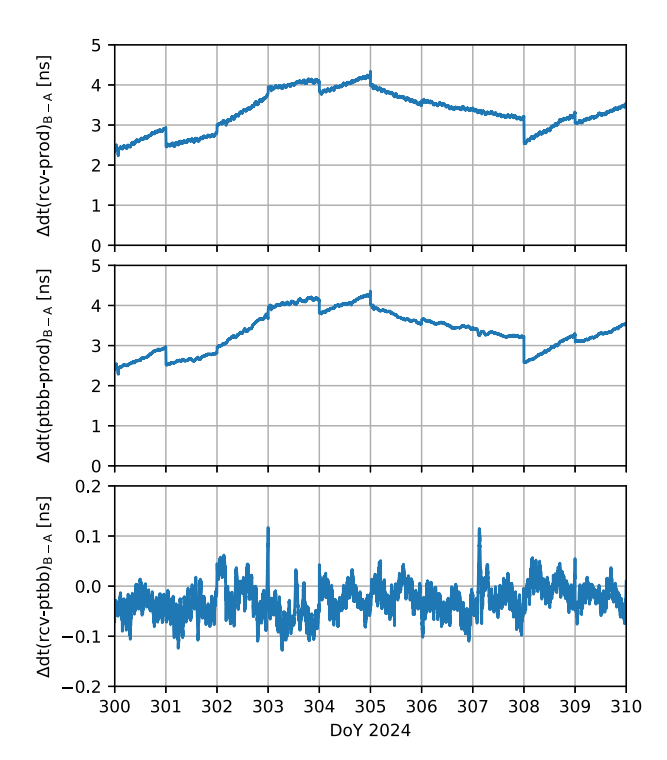


Fig. 7. Differences B–A of clock offset derived in processing chains A (DLR) and B (ESA). Top: S6A receiver clock offset from the time scale of the GNSS orbit/clock product; center: PTBB receiver time offset from the GNSS product system time scale; bottom: S6A receiver clock offset from UTC(PTB).

ences of S6A-UTC(PTB) clock offset estimates of chains B and A amount to 0.04 ns (1.5 cm) over the 10-day test period, which includes a standard deviation of 0.03 ns (1 cm) and a (negative) bias of the same magnitude. This bias can be attributed to the different scale of the IGS20 and ESA23 antenna models, which induces a station height offset of about 6–7 mm along with a corresponding clock offset. The remainder might relate to different tropospheric delay models/estimates as well as a small offset in the mean orbital radius of S6A caused by the different force models in the two POD systems.

Even though the consistency of the two processing chains might be further improved through careful tuning and model harmonization, the "as-is" comparison is considered to offer a fair measure of the accuracy and precision of LEO-to-ground time transfer that can be expected with state-of-the-art POD/PPP systems. With representative uncertainties at the 1-cm level, the proposed methodology is thus well suited to assess the performance of GNSS-based onboard time synchronization with expected performances at the decimeter level.

5.4. Onboard time assessment

Upon combining the LEO receiver clock offset as estimated by an onboard navigation system with the ground-based determination of the LEO receiver clock offset from a UTC(k) laboratory or similar reference, the offset of the

onboard time scale from UTC and related terrestrial time scales can be determined. This is illustrated in Fig. 8 for the (simulated) S6A real-time navigation solution presented in Section 5.2. Over the 10-day analysis period considered for this study, the difference between the onboard time scale and UTC(PTB) varies in a range of roughly -4 - +2 ns. This comprises both stochastic variations at the 1-ns level over sub-daily time scales as well as a roughly quadratic trend covering a range of about 3 ns. The latter can largely be attributed to the long-term variation of the difference between UTC(PTB) and GST in the period of interest, which is shown in the central part of Fig. 8. When evaluating the onboard time offset from GST, the previously observed trend is indeed fully removed and the onboard time is found to agree with GST at the level of 0.75 ns or 23 cm (RMS) with a mean offset of 0.015 ns (0.5 cm).

The spectral characteristics of the S6A onboard time offset from Galileo System Time (GST) are, furthermore, illustrated by the time deviation (TDEV) represented in Fig. 9. It shows a roughly monotonic increase from a few hundredths of a nanosecond at the 30 s sampling interval of the ONS to a few tenths of a nanosecond at time scales of several hours. A local maximum of roughly 0.35 ns is attained at time intervals of about 55 min corresponding to half the orbital period. It reflects the presence of orbit-periodic errors in the real-time navigation solution, which are a well-known feature in satellite orbit determination

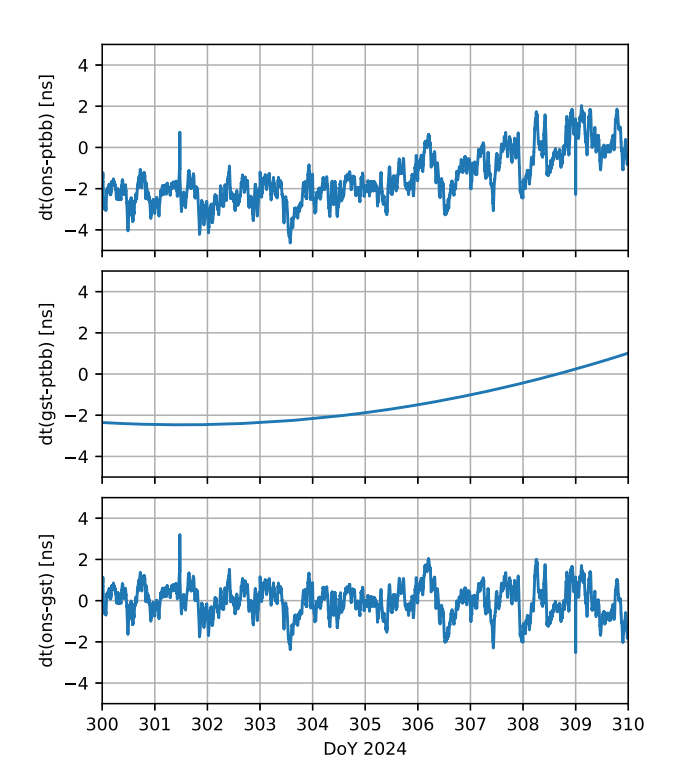


Fig. 8. Offset of the S6A onboard time as established by the (playback) real-time navigation system from UTC(PTB) (top) and from Galileo System Time (GST; bottom). The center figure shows the GST-UTC(PTB) time offset used to translate between both time scales.

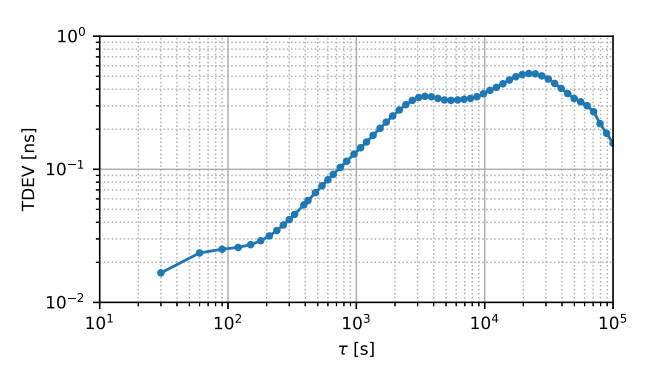


Fig. 9. Time deviation (TDEV) of the S6A onboard time offset from Galileo System Time (GST) as a function of the time interval τ .

(Colombo, 1989) and likewise affect the onboard clock estimation. This is followed by a global maximum of about 0.5 ns close to the semi-period of the GNSS constellations.

The analysis confirms that broadcast navigation data can provide an unbiased access to Galileo System Time, which is itself aligned to UTC at a level of one or a few nanoseconds. In terms of stability, the onboard time scale determined with the sample real-time navigation system used for the present study exhibits a roughly 2-3 times higher scatter than the LEO satellite position. This apparent inconsistency can largely be attributed to the fact that carrier phase observations allow for sensing position changes in a real-time navigation system with a precision that is largely driven by the signal-in-space range error of the broadcast ephemerides. The clock offset determination, on the other hand, suffers from a notable correlation with the carrier phase ambiguities due to the fairly short tracking arcs encountered in low Earth orbit and is therefore subject to higher uncertainties than the estimation of the position components. Further improvements of the onboard time scale obtained in a GNSS-based real-time navigation can be expected from the use of correction services such as the Galileo High Accuracy Service (HAS) to reduce the broadcast ephemeris error (Hauschild et al., 2022; Sun et al., 2025). However, these are beyond the scope of the present study, which focuses on the verification and monitoring of the onboard time rather than its actual improvement.

6. Summary and conclusions

A conceptual framework for comparing a GNSS-based LEO onboard time scale realization with a global time reference scale on ground is presented and discussed. It resembles established concepts for PPP time transfer between terrestrial receivers, but replaces the kinematic positioning of the orbiting receiver by a reduced-dynamic precise orbit determination. The concept addresses a key element for validating the onboard synchronization of navigation signals transmitted by future LEO-PNT constellations. Necessary input data comprise pseudorange and carrier phase observations from the LEO GNSS receiver with consistent

time tags $t_{rev(leo)}$ in the LEO receiver time scale, and the LEO receiver clock offset $dt_{rev(leo),ons}$ obtained by the onboard navigation system from the above observations, both of which must be available through the onboard telemetry. These must be complemented with the known biases of the LEO antenna-receiver chain for delay correction and information to what extend those corrections have been considered in the receiver-internal measurement generation and the onboard navigation system as well as information on the type of relativistic corrections (if any) considered in the definition of the ONS time scale and the computation of the $dt_{rcv(leo),ons}$ clock offset values. Aside from that, GNSS observations of a suitable time reference station (e.g., a UTC(k) laboratory or a GNSS receiver connected to the master clock of a GNSS provider) along with total delay calibrations are required that offer GNSS-based access to either a laboratory-specific UTC(k) or a GNSS system time scale. The precise orbit, clock, and bias products for the GNSS jointly observed by the LEO and TRS receivers serve as a catalyst for the LEO-to-ground time transfer and are readily available from various IGS analysis centers. The three-way comparison of time-offsets (LEO GNSS receiver vs. LEO ONS, LEO GNSS receiver vs precise GNSS product, and UTC/GNSS time vs. precise GNSS product) then enables the monitoring of the LEO onboard time scale relative to UTC or a GNSS system time scale.

Based on Galileo and GPS observations of the Sentinel-6A satellite along with the respective broadcast ephemerides, the feasibility of synchronizing the LEO onboard time with UTC or Galileo system time at a precision of about 0.75 ns (23 cm) is demonstrated using a representative play-back navigation filter. Compared to a 9 cm 3D RMS position error achieved in the same real-time navigation process, the resulting onboard time knowledge is roughly a factor of 2-3 worse. This performance difference appears as a general feature of GNSS-based onboard navigation systems, which can fully exploit the precision of carrier phase observations for positioning but suffer from the correlation of clock offsets and phase ambiguities in the parameter estimation. On the other hand further improvements may be expected from the use real-time correction services such as the Galileo HAS as well as carrier phase ambiguity resolution in the onboard navigation process ephemeris error.

The monitoring of the onboard time itself can be performed with a precision of 0.05 ns $(1-2 \, \mathrm{cm})$ as derived from the comparison of two fully independent processing chains for the space-to-ground time transfer. Calibration uncertainties of the GNSS receiving chain at the time reference station may contribute systematic errors at the 0.1 ns level. On the other hand the realization and determination of the onboard time scale depends on the knowledge of time- and temperature-dependent biases in the LEO GNSS receiver system, including the antenna, low-noise amplifier, reference oscillator, and front-end, as well as possible

digital delays in the signal-processing. A careful calibration of these contributions appears essential to achieve a proper a priori synchronization of a LEO-PNT time scale with UTC or GNSS time.

Data availability

GNSS observations files, broadcast ephemerides, and precise orbit/clock products as used in the study are publicly available from data centers of the International GNSS Service, including CDDIS (https://cddis.nasa.gov/archive/gnss/data/) and GSSC (https://gssc.esa.int). Precise orbit and clock products of the ESOC analysis center are made available through the Navigation Office website at http://navigation-office.esa.int/products/. Sentinel-6A GNSS observations and auxiliary data for POD are openly shared at the Copernicus Data Space Ecosystem (https://dataspace.copernicus.eu).

Declaration of Competing Interest

The authors declare that they have no known competing financial interests or personal relationships that could have appeared to influence the work reported in this paper.

Acknowledgments

GNSS observation data and navigation messages used in this study were kindly provided by the international GNSS Service (IGS). The support of all station providers, analysis centers and data centers is gratefully acknowledged. The authors would, furthermore, like to thank Pietro Giordano, Volker Mayer, Michiel Otten, and Erik Schönemann for technical support and discussion during the study performance and the preparation of the manuscript.

References

Anderson, P., 2023. Trustpoint system/service overview. In International Committee on Global Navigation Satellite Systems (ICG) Workshop on Low Earth Orbit (LEO) Positioning Navigation and Timing (PNT) Systems. UNOOSA, URL: https://www.unoosa.org/documents/pdf/icg/2023/ICG_WG-S_LEO-PNT_Workshop_June_2023/ICG_LEO-PNT_Workshop_2023_03.pdf.

Bar-Sever, Y., 2021. Orbit determination with GNSS. In: Y.T.J. Morton, F. van Diggelen, J. J. J. Spilker, & P.B.W (Eds.), Position, Navigation, and Timing Technologies in the 21st Century: Integrated Satellite Navigation, Sensor Systems, and Civil Applications chapter 62. (pp. 1893–1919). Wiley IEEE Press volume 2. doi: https://doi.org/10.1002/9781119458555.ch62.

BIBM, 2024. 2022 Group 1 GNSS calibration trip (Cal_Id 1001–2022) Summary, v1.1, Bureau International des Poids et Mesure, 16 May 2024. https://webtai.bipm.org/ftp/pub/tai/publication/time-calibration/Current/1001-2022_GPSP3C1-GALE3-BDSB3_Group1-trip_V1-1 pdf

BIBM, 2025. BIPM time department data base. https://webtai.bipm.org/database/calib.html.

- Calliess, D., Montenbruck, O., Wermuth, M., et al., 2024. Long-term analysis of Sentinel-6A orbit determination: Insights from three years of flight data. Adv. Space Res. 74 (7), 3011–3027. https://doi.org/10.1016/j.asr.2024.06.043.
- Chen, L., Lv, F., Yang, Q., et al., 2023. Performance evaluation of CentiSpace navigation augmentation experiment satellites. Sensors 23 (12), 5704. https://doi.org/10.3390/s23125704.
- Colombo, O.L., 1989. The dynamics of global positioning system orbits and the determination of precise ephemerides. J. Geophys. Res.: Solid Earth 94 (B7), 9167–9182. https://doi.org/10.1029/JB094iB07p09167.
- Dach, R., Schaer, S., Arnold, D. et al., 2023. CODE final product series for the IGS. URL: http://www.aiub.unibe.ch/download/CODE. doi: https://doi.org/10.48350/185744.
- Darugna, F., Casotto, S., Bardella, M. et al., 2022. Sentinel-6A GPS and Galileo dual-frequency real-time reduced-dynamics P2OD. In 10th Workshop on Satellite Navigation Technology (NAVITEC 2022) (pp. 1–12). IEEE. doi: https://doi.org/10.1109/NAVITEC53682.2022. 9847561.
- De Gaudenzi, R., 2025. An integrated LEO communication and PNT system for beyond 5G NTN. Int. J. Satell. Commun. Network. 43, 293–308.
- Defraigne, P., Petit, G., 2015. CGGTTS-Version 2E: an extended standard for GNSS time transfer. Metrologia 52 (6), G1. https://doi. org/10.1088/0026-1394/52/6/G1.
- Delporte, J., Mercier, F., Laurichesse, D., et al., 2008. GPS carrier-phase time transfer using single-difference integer ambiguity resolution. Int. J. Navigat. Observ. 2008 (1), 273785. https://doi.org/10.1155/2008/ 273785.
- Donlon, C.J., Cullen, R., Giulicchi, L., et al., 2021. The Copernicus Sentinel-6 mission: Enhanced continuity of satellite sea level measurements from space. Remote Sens. Environ. 258, 112395. https://doi.org/ 10.1016/j.rse.2021.112395.
- Eissfeller, B., Pany, T., Dötterböck, D., et al., 2024. A comparative study of LEO-PNT systems and concepts. In: Proceedings of the ION 2024 Pacific PNT Meeting, pp. 758–782. https://doi.org/10.33012/ 2024.19646.
- Elwischger, B.P.B., Thoelert, S., Suess, M. et al., 2013. Absolute calibration of dual frequency timing receivers for Galileo. In: Proceedings of the European Navigation Conference, ENC 2013, Vienna.
- Fernandez, J., Peter, H., Fernandez, C., et al., 2024. The Copernicus POD service. Adv. Space Res. 74 (6), 2615–2648. https://doi.org/10.1016/j. asr.2024.02.056.
- Gini, F., Mayer, V., Traiser, B., et al., 2024. Advancements in operational gnss processing: A comprehensive analysis of ESA's new methodology.
 In: 9th International Colloquium on Scientific and Fundamental Aspects of GNSS, Poland, 25–27 Sept. 2024. ESA. Wrocław.
- Giordano, P., Zoccarato, P., Walker, R. et al., 2018. ESA activities and plans for experimentation and exploitation of precise real-time onboard orbit determination (P2OD). In NAVITEC 2018, 5 - 7 December 2018, ESA-ESTEC. ESA.
- Hauschild, A., 2017. Basic observation equations. In: Teunissen, P., Montenbruck, O. (Eds.), Springer Handbook of Global Navigation Satellite Systems chapter, 19. Springer, pp. 561–582. https://doi.org/ 10.1007/978-3-319-42928-1 19.
- Hauschild, A., Montenbruck, O., 2021. Precise real-time navigation of LEO satellites using GNSS broadcast ephemerides. NAVIGATION: J. Inst. Navig. 68 (2), 419–432. https://doi.org/10.1002/navi.416.
- Hauschild, A., Montenbruck, O., Steigenberger, P., et al., 2022. Orbit determination of Sentinel-6A using the Galileo high accuracy service test signal. GPS Solutions 26 (4), 120. https://doi.org/10.1007/s10291-022-01312-5.
- Iannucci, P.A., Humphreys, T.E., 2022. Fused low-Earth-orbit GNSS. IEEE Trans. Aerosp. Electron. Syst. 60 (4), 3730–3749. https://doi. org/10.1109/TAES.2022.3180000.
- Johnston, G., Riddell, A., Hausler, G., 2017. The International GNSS Service. In: Teunissen, P., Montenbruck, O. (Eds.), Springer Hand-

- book of Global Navigation Satellite Systems chapter, 33. Springer, pp. 967–982. https://doi.org/10.1007/978-3-319-42928-1 33.
- Kouba, J., 2002. Relativistic time transformations in GPS. GPS Solutions 5 (4), 1–9. https://doi.org/10.1007/PL00012907.
- Kouba, J., 2004. Improved relativistic transformations in GPS. GPS Solutions 8, 170–180. https://doi.org/10.1007/s10291-004-102-x.
- Kunzi, F., Braun, B., Markgraf, M., et al., 2023. A GNSS-synchronized satellite navigation payload for LEO PNT. In: Proceedings ION GNSS+ 2023, pp. 1425–1435. https://doi.org/10.33012/2023.19322.
- Kunzi, F., Montenbruck, O., 2022. Precise on-board clock synchronization for LEO satellites. NAVIGATION J. ION 69 (3), navi.531. https://doi.org/10.33012/navi.5.
- Langley, R., Teunissen, P., Montenbruck, O., 2017. Introduction to GNSS. In: Teunissen, P., Montenbruck, O. (Eds.), Springer Handbook of Global Navigation Satellite Systems chapter, 1. Springer, pp. 3–23. https://doi.org/10.1007/978-3-319-42928-1_1.
- Larson, K.M., Ashby, N., Hackman, C., et al., 2007. An assessment of relativistic effects for low Earth orbiters: the GRACE satellites. Metrologia 44 (6), 484. https://doi.org/10.1088/0026-1394/44/6/007.
- Le Priellec, A., Giordano, P., Limon, M.C. et al., 2025. LEO-PNT end-to-end in-orbit demonstration: an ESA initiative to pave the way for a European GNSS constellation in LEO. In Small Satellites Systems and Services Symposium (4S 2024) (pp. 1304–1312). SPIE volume 13546. https://doi.org/10.1117/12.3062635.
- Li, M., Qin, G., Jiang, K., et al., 2023. Performance assessment of real-time orbit determination for the Haiyang-2D using onboard BDS-3/GPS observations. Adv. Space Res. 71 (3), 1657–1669. https://doi.org/10.1016/j.asr.2022.09.050.
- Li, W., Yang, Q., Du, X., et al., 2024. LEO augmented precise point positioning using real observations from two CENTISPACETM experimental satellites. GPS Solutions 28 (1), 44. https://doi.org/ 10.1007/s10291-023-01589-0.
- Menzione, F., Paonni, M., 2023. LEO-PNT mega-constellations: a new design driver for the next generation MEO GNSS space service volume and spaceborne receivers. In: In 2023 IEEE/ION Position, Location and Navigation Symposium (PLANS). IEEE, pp. 1196–1207. https:// doi.org/10.1109/PLANS53410.2023.10140052.
- Montenbruck, O., Hackel, S., Wermuth, M., et al., 2021. Sentinel-6A precise orbit determination using a combined GPS/Galileo receiver. J. Geodesy 95 (9), 109. https://doi.org/10.1007/s00190-021-01563-z.
- Montenbruck, O., Kunzi, F., Hauschild, A., 2022. Performance assessment of GNSS-based real-time navigation for the Sentinel-6 spacecraft. GPS Solutions 26 (1), 12. https://doi.org/10.1007/s10291-021-01198-9.
- Montenbruck, O., Steigenberger, P., 2022. BRD400DLR: DLR's merged multi-GNSS broadcast ephemeris product in RINEX 4.00 format; DLR/GSOC. https://doi.org/10.57677/BRD400DLR.
- Mu, X., 2023. CENTISPACE LEO augmentation navigation system status. In International Committee on Global Navigation Satellite Systems (ICG) Workshop on Low Earth Orbit (LEO) Positioning Navigation and Timing (PNT) Systems. UNOOSA., URL: https://www.unoosa.org/documents/pdf/icg/2023/ICG_WG-S_LEO-PNT_Workshop_June_2023/ICG_LEO-PNT_Workshop_2023_01.pdf.
- Peter, H., Springer, T., Zangerl, F., et al., 2022. Beyond Gravity PODRIX GNSS receiver on Sentinel-6 Michael Freilich–receiver performance and POD analysis. In: Proceedings ION GNSS+ 2022, pp. 589–601. https://doi.org/10.33012/2022.18368.
- Petit, G., Jiang, Z., Uhrich, P., et al., 2000. Differential calibration of Ashtech Z12-T receivers for accurate time comparisons. In: Proc. 14th European Frequency and Time Forum, pp. 40–44.
- Petit, G., Kanj, A., Loyer, S., et al., 2015. 1×10^{-16} frequency transfer by GPS PPP with integer ambiguity resolution. Metrologia 52 (2), 301. https://doi.org/10.1088/0026-1394/52/2/30.
- Petit, G., Luzum, B., 2010. IERS Conventions (2010), Technical Note No. 36. Frankfurt: Bundesamt für Kartographie und Geodäsie.

- Proia, A., Cibiel, G., White, J., et al., 2011. Absolute calibration of GNSS time transfer systems: NRL and CNES techniques comparison. https://doi.org/10.1109/FCS.2011.5977799.
- Prol, F.S., Ferre, R.M., Saleem, Z., et al., 2022. Position, navigation, and timing (PNT) through low Earth orbit (LEO) satellites: A survey on current status, challenges, and opportunities. IEEE Access 10, 83971–84002. https://doi.org/10.1109/ACCESS.2022.3194050.
- Reid, T.G., Neish, A.M., Walter, T., et al., 2018. Broadband LEO constellations for navigation. NAVIGATION J. ION 65 (2), 205–220. https://doi.org/10.1002/navi.234.
- Ries, L., Limon, M.C., Grec, F.-C., et al., 2023. LEO-PNT for augmenting europe's space-based PNT capabilities. In: In 2023 IEEE/ION Position, Location and Navigation Symposium (PLANS). IEEE, pp. 329–337. https://doi.org/10.1109/PLANS53410.2023. 10139999.
- Riley, C., 2023. High-performance and resilient PNT (position, navigation & timing). In: In International Committee on Global Navigation Satellite Systems (ICG) Workshop on Low Earth Orbit (LEO) Positioning Navigation and Timing (PNT) Systems. UNOOSA, URL: https://www.unoosa.org/documents/pdf/icg/2023/ICG_WGS_LEO-PNT_Workshop_June_2023/ICG_LEO-PNT_Workshop_2023_05.pdf.
- Romero, I., 2017. RINEX the receiver independent exchange format, version3.03, 25 January 2017, International GNSS Service (IGS), RINEX Working Group and Radio Technical Commission for Maritime Services Special Committee 104 (RTCM-SC104). https://files.igs.org/pub/data/format/rinex303_update1.pdf.
- Springer, T.A., 2009. NAPEOS mathematical models and algorithms, DOPS-SYS-TN-0100-OPS-GN, ESA/ESOC, Darmstadt.
- Stock, W., Schwarz, R.T., Hofmann, C.A., et al., 2025. Survey on opportunistic PNT with signals from LEO communication satellites. IEEE Commun. Surv. Tutor. 27 (1), 77. https://doi.org/10.1109/ COMST.2024.3406990.
- Sun, S., Chai, H., Wang, M., et al., 2025. POD performance of LEO satellites with Galileo high accuracy service (HAS) of initial service

- phase. Adv. Space Res. 75 (6), 4963–4976. https://doi.org/10.1016/j.asr.2024.12.062.
- Teunissen, P.J., 2021. GNSS precise point positioning. In Y.T.J. Morton, F. van Diggelen, J. J. J. Spilker, & P.B.W (Eds.), Position, Navigation, and Timing Technologies in the 21st Century: Integrated Satellite Navigation, Sensor Systems, and Civil Applications chapter 20. (pp. 503–528). Wiley IEEE Press volume 1. https://doi.org/10.1002/9781119458555.ch20.
- Valat, D., Delporte, J., 2020. Absolute calibration of timing receiver chains at the nanosecond uncertainty level for GNSS time scales monitoring. Metrologia 57 (2), 025019. https://doi.org/10.1088/1681-7575/ab57f5.
- Van Uytsel, W., Janssen, T., Weyn, M., et al., 2024. A technical overview of current "New Space" LEO-PNT initiatives and their application potential. In: Proceedings 35th International Symposium on Personal, Indoor and Mobile Radio Communications (IEEE/PIMRC). IEEE. https://doi.org/10.1109/PIMRC59610.2024.10817274.
- Waller, P., Valceschini, R., Delporte, J., et al., 2019. Cross-calibrations of multi-GNSS receiver chains. In: In 2019 Joint Conference of the IEEE International Frequency Control Symposium and European Frequency and Time Forum (EFTF/IFC), pp. 1–4. https://doi.org/ 10.1109/FCS.2019.8856134.
- Wolf, P., Petit, G., 1995. Relativistic theory for clock syntonization and the realization of geocentric coordinate times. Astron. Astrophys. 304, 653
- Youn, C., 2023. XONA Space Systems. In International Committee on Global Navigation Satellite Systems (ICG) Workshop on Low Earth Orbit (LEO) Positioning Navigation and Timing (PNT) Systems. UNOOSA, URL: https://www.unoosa.org/documents/pdf/icg/2023/ ICG_WG-S_LEO-PNT_Workshop_June_2023/ICG_LEO-PNT_ Workshop_2023_04.pdf.
- Young, L., 2017. JPL GNSS receivers, past, present, and future. In SCaN/ HEOMD Workshop on Emerging Technologies for Autonomous Space Navigation. NASA, https://hdl.handle.net/2014/47433.